Volume 2
Number 4
July 2025
Pages 843–1092

RSC Applied Interfaces

rsc.li/RSCApplInter

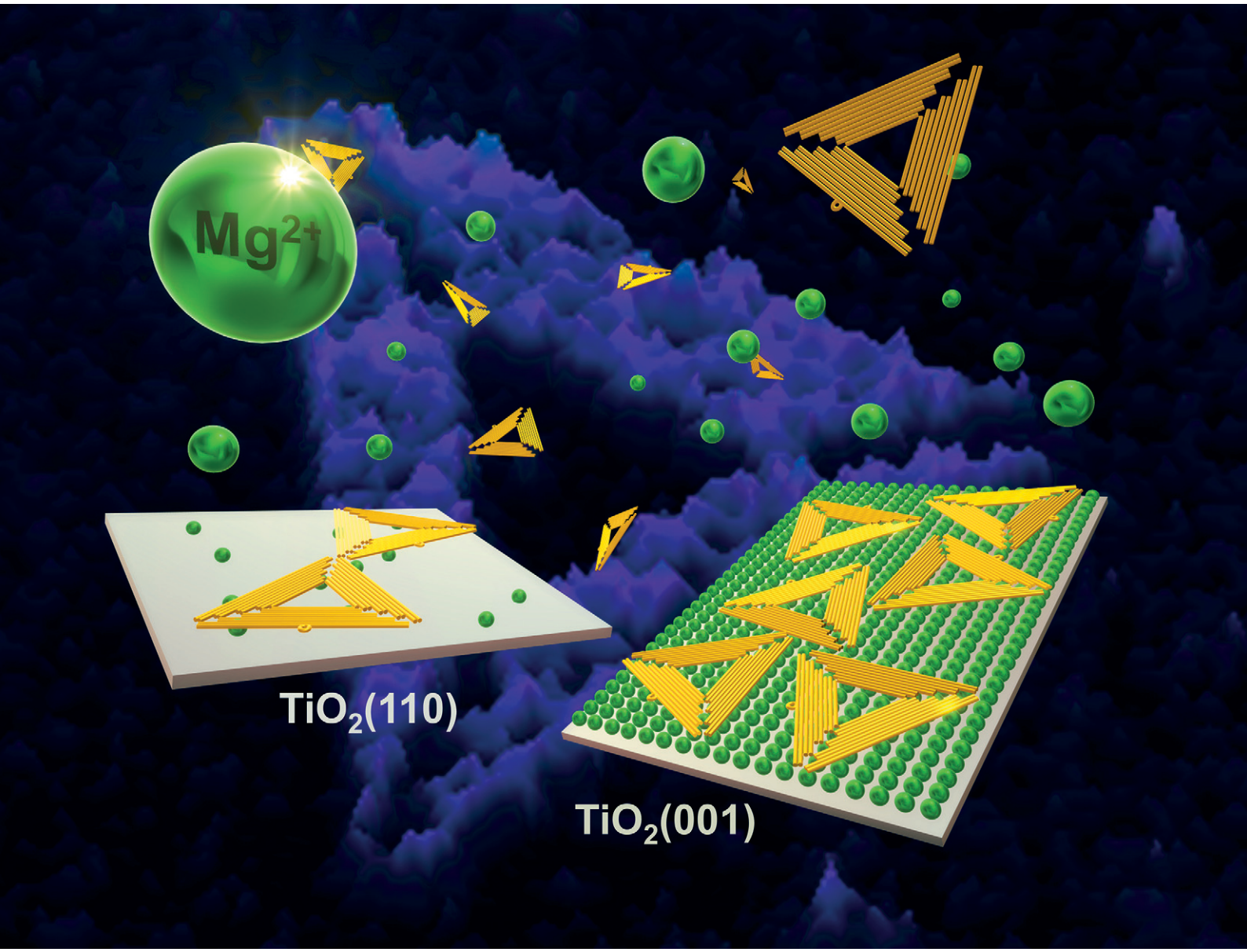

ISSN 2755-3701

ROYAL SOCIETY OF CHEMISTRY

PAPER
Adrian Keller *et al.*
DNA origami adsorption at single-crystalline TiO_2 surfaces

RSC Applied Interfaces

ROYAL SOCIETY OF CHEMISTRY

PAPER

View Article Online
View Journal | View Issue

Cite this: *RSC Appl. Interfaces*, 2025, **2**, 931

DNA origami adsorption at single-crystalline TiO_2 surfaces†

Xiaodan Xu, Sandra Gołębiowska, Teresa de los Arcos, Guido Grundmeier and Adrian Keller *

The immobilization of DNA origami nanostructures on solid surfaces is an important prerequisite for their application in many biosensors. So far, DNA origami immobilization has been investigated in detail only on a few surfaces such as mica, SiO_2, and graphite. TiO_2 is a conductive oxide with extensive applications in photocatalysis, energy conversion, and (bio)sensing. Despite its great importance, however, TiO_2 has not been investigated as a substrate for DNA origami immobilization yet. Here, we systematically investigate the adsorption of 2D DNA origami triangles on single-crystalline TiO_2 surfaces under various experimental conditions. Interestingly, the effect of the Mg^{2+} concentration on DNA origami surface coverage is found to depend on the orientation of the TiO_2 surface. On TiO_2(110) and TiO_2(111), 10 mM Mg^{2+} yields a higher surface coverage than 5 mM. However, the inverse is observed for the TiO_2(001) surface, where the lower Mg^{2+} concentration leads to an increase in surface coverage by up to 75%. This is explained by the interplay between Mg^{2+} binding to the DNA phosphates and Mg^{2+} adsorption at the TiO_2 surfaces, which in the case of TiO_2(001) results in a maximum density of Mg^{2+} salt bridges already at a low Mg^{2+} concentration. At higher concentrations, both the surface and the DNA phosphates are getting saturated with Mg^{2+} ions, which introduces electrostatic repulsion at the TiO_2–DNA interface and thus lowers the surface coverage. Our results demonstrate that DNA origami surface coverage at different TiO_2 surfaces can be controlled by the Mg^{2+} concentration. However, the same mechanism may also play a role in DNA origami adsorption at other single-crystalline oxide surfaces.

Received 15th April 2025,
Accepted 15th May 2025

DOI: 10.1039/d5lf00109a

rsc.li/RSCApplInter

Introduction

DNA origami nanostructures[1] have become a widely employed molecular tool in biosensing.[2–5] These nanostructures are fabricated by folding a single-stranded DNA scaffold into an arbitrary, user-defined shape *via* hybridization with a set of short synthetic oligonucleotides called staple strands.[6,7] It allows for the precise fabrication of two- and three-dimensional nanostructures, which can be modified with sub-nanometer precision to display controlled arrangements of DNA motifs,[8] small molecule ligands,[9] antibodies,[10] enzymes,[11] fluorescent dyes,[12] and various inorganic nanoparticles.[13–17] This versatility is exploited in various biosensor concepts, in which the DNA origami nanostructures may serve as both recognition elements and transducers. DNA origami biosensors can therefore implement diverse detection strategies based on fluorescence,[17] surface-enhanced Raman scattering,[18] circular dichroism,[14] surface plasmon resonance,[19] and electrochemistry,[20] among others. Since many sensor concepts require the immobilization of the DNA origami nanostructures on solid surfaces, controlling DNA origami adsorption at relevant materials interfaces has become an important technological issue.[21–31] Most of the previous works focused on SiO_2 surfaces,[21,23–26,28,30,31] while a few investigated also carbon-based materials.[22,27,29]

TiO_2 has unique photocatalytic and electronic properties, making it a key candidate for diverse applications such as environmental remediation, photovoltaics, and sensing. TiO_2 is used as a photocatalyst in water splitting,[32–34] in CO_2 reduction,[35–37] and in solar hydrogen[38] and energy harvesting[39] strategies, thus playing a crucial role in sustainable energy solutions. Furthermore, its high surface reactivity, stability, and tunable electronic properties under ultraviolet (UV) light irradiation render TiO_2 a highly interesting material for the development of sensors for the detection of gases, chemicals, and biological molecules.[40–42] For such applications, understanding and ultimately controlling the interaction of TiO_2 surfaces with relevant molecules is an important factor. Biomolecules have received particular attention in this regard because of the

Technical and Macromolecular Chemistry, Paderborn University, Warburger Str. 100, Paderborn 33098, Germany. E-mail: adrian.keller@uni-paderborn.de

† Electronic supplementary information (ESI) available: Contact angle measurements; additional AFM images with and without applied thresholds; XPS results. See DOI: https://doi.org/10.1039/d5lf00109a

important applications of TiO_2-based materials in biosensing as well as regenerative medicine. Most studies in this area have focused on proteins because of their ubiquitous presence in physiological media and their great relevance as diagnostic biomarkers.[43–50] However, there are also DNA-based sensing concepts utilizing TiO_2 surfaces, nanoparticles, and nanowires.[51–60]

Despite its great importance in biosensing and biomedicine, TiO_2 so far has not been investigated as a substrate for DNA origami adsorption. This study aims to close this gap and investigates the adsorption of two-dimensional DNA origami triangles at single-crystalline TiO_2 surfaces. Atomic force microscopy (AFM) is used to quantify DNA origami surface coverage in dependence of the DNA origami and Mg^{2+} concentrations, as well as the incubation time. We observe that DNA origami adsorption is influenced by the orientation of the TiO_2 surface, with the TiO_2(001) surface exhibiting a higher DNA origami surface coverage at 5 mM than at 10 mM Mg^{2+}. For TiO_2(110) and TiO_2(111), the situation is reversed. These observations are attributed to the interplay between Mg^{2+} binding to the DNA and Mg^{2+} adsorption at the TiO_2 surfaces, which is stronger on the TiO_2(001) surface due to its larger content of surface oxygens resulting in increased basicity.

Materials and methods

DNA origami assembly and purification

DNA origami triangles[1] were assembled using the single-stranded M13mp18 scaffold DNA (BAYOU BIOLABS) and 208 staple strands (Eurofins). The staples and scaffold were mixed at a 10 : 1 molar ratio in 1× TAE buffer (pH 8.5, Carl Roth) supplemented with 10 mM $MgCl_2$ (Carl Roth) in a 100 μL reaction volume. The mixture was placed in a thermocycler (Primus 25 Advanced, PEQLAB), heated to 80 °C, gradually cooled to room temperature, and stored at 4 °C. To remove the unbound staples, the samples were purified using 100 kDa molecular weight cutoff filters (Amicon Ultra, Millipore) with 1× TAE supplemented with 10 mM $MgCl_2$ as the solvent. For Mg^{2+}-free experiments, the assembly buffer was exchanged during spin filtering against Mg^{2+}-free Tris buffer (40 mM, pH 8.5) as described previously,[61] resulting in a residual Mg^{2+} concentration around 10 μM. A UV-vis spectrophotometer (Implen Nanophotometer P330) was used to measure the concentration of assembled DNA origami nanostructures based on their absorption at 260 nm.[62]

Substrate preparation

TiO_2(001), TiO_2(110), and TiO_2(111) wafers were purchased from Crystal GmbH. The substrates were soaked in Hellmanex III solution (Hellma GmbH) for two hours, rinsed thoroughly with HPLC-grade water (Carl Roth) and subsequently dried under a stream of argon. The cleaned substrates were treated with an O_2 plasma (Diener Zepto, Diener Electronic) for 1 minute to create a hydrophilic, hydroxyl-rich surface.[63] This was verified by contact angle measurements (see Fig. S1†). Afterwards, the substrates were examined using AFM. If contaminants were detected in the AFM images, the cleaning process was repeated until a clean surface was achieved.

Si(100) wafers (Siegert Wafer) with native surface oxide were immersed in preheated RCA-1 solution (1 : 1 : 5 25% NH_3, 35% H_2O_2, H_2O) at 75 °C for 15 min to remove organic residues and create a hydrophilic hydroxyl-rich surface.[64] Then, they were rinsed thoroughly with HPLC-grade water and subsequently dried with stream of argon.

Contact angle measurements

The contact angle measurements were performed using an OCA 15 plus contact angle system (Dataphysics Instruments) with the sessile drop method, applying 5 μl of HPLC-grade water (Carl Roth) on the surface.

DNA origami adsorption

The assembled DNA origami triangles were diluted to concentrations of 0.5 nM, 1 nM, 2.5 nM, and 5 nM in 1× TAE buffer supplemented with 5 mM and 10 mM $MgCl_2$, respectively. For Mg^{2+}-free experiments, the samples were diluted in pure Tris buffer. 50 μL samples were pipetted onto the substrates and incubated for 1, 5, 10, and 30 minutes, respectively. After incubation, the substrates were gently rinsed with HPLC-grade water and dried under a stream of argon.

AFM imaging

AFM imaging was performed in air using a Bruker Dimension Icon operated in ScanAsyst mode with SCANASYST-AIR cantilevers (Bruker) with a nominal tip radius of 2 nm and a JPK Nanowizard 3 operated in intermittent contact mode with HQ:NSC18/Al BS cantilevers (MikroMasch) with a tip radius <8 nm. Images were acquired with a scan size of 2 × 2 μm^2 at a resolution of 1024 × 1024 pixels.

Image processing

The images were processed using the open-source software Gwyddion.[65] To calculate the DNA origami surface coverage, a suitable height threshold was applied to each image using the Mark by Threshold tool. The value of the threshold was adjusted individually for each image to mask only the DNA origami nanostructures but not the surface. The surface coverage was subsequently calculated using the Grain Summary tool.

X-ray photoelectron spectroscopy (XPS)

XPS measurements were conducted in ultra-high vacuum (base pressure better than 10^{-10} mbar) using an Omicron ESCA+ system (Omicron NanoTechnology) with a monochromatic Al Kα (1486.7 eV) X-ray source and a hemispherical energy analyzer. The source-analyzer angle was 102°, while the take-off angle of the detected photoelectrons was set to 30° with respect to the surface plane. A pass energy of 100 eV, a step size of 0.5 eV, and a dwell time of 0.1 s were used for survey spectra. A

pass energy of 20 eV, a step size of 0.1 eV, and a dwell time of 0.5 s were used for high-resolution core-level spectra. Neutralization was done using simultaneous irradiation with a low energy electron beam (2 eV). The O 1s peaks were fitted using the UNIFIT 2019 program, using a convolution of Gaussian and Lorentzian line shapes and Shirley-type backgrounds. In the fit, the Lorentzian component was fixed to 0.1 eV, while the Gaussian width was left free. The stoichiometry was determined by the normalization to 100% of the background-subtracted areas divided by the appropriate normalization factors.

Results and discussion

DNA adsorption at TiO_2 surfaces has mostly been studied at acidic pH close to or below the isoelectric point (IEP) of the TiO_2 surface.[59,60,66] Under such conditions, the TiO_2 surface is electrically neutral or positively charged, so that there is no electrostatic repulsion between the surface and the negatively charged DNA. DNA origami nanostructures, however, are usually synthesized in TAE buffer with a pH of 8.5, at which the TiO_2 surface is negatively charged.[67] Therefore, adsorption of the negatively charged DNA origami nanostructures at this pH requires the presence of a sizeable amount of divalent cations in solution to act as salt bridges at the TiO_2–DNA interface. Mg^{2+} ions are the most obvious candidates for this as they are usually added to the TAE buffer during DNA origami assembly to screen electrostatic interhelix repulsion.[68] To verify the role of salt bridges in DNA origami adsorption at TiO_2 surfaces, assembled DNA origami triangles (2.5 nM) were transferred into pure Tris buffer (pH 8.5, residual Mg^{2+} concentration about 10 μM)[61] and incubated for 10 min on the TiO_2(001) surface (IEP 5.5–5.8).[67] As can be seen in the AFM image shown in Fig. S3,† no DNA origami triangles are detected on the surface after incubation. In contrast, incubation under equivalent conditions but in the presence of 5 mM Mg^{2+} leads to a large number of adsorbed DNA origami triangles (see Fig. 1), which supports the assumption that DNA origami adsorption at the TiO_2(001) at basic pH requires salt bridges. Therefore, we investigated the adsorption of DNA origami triangles at the TiO_2(001) surface for different Mg^{2+} concentrations of 5 mM and 10 mM, different DNA origami concentrations between 0.5 and 5 nM, and different incubation times between 1 min and 30 min, respectively.

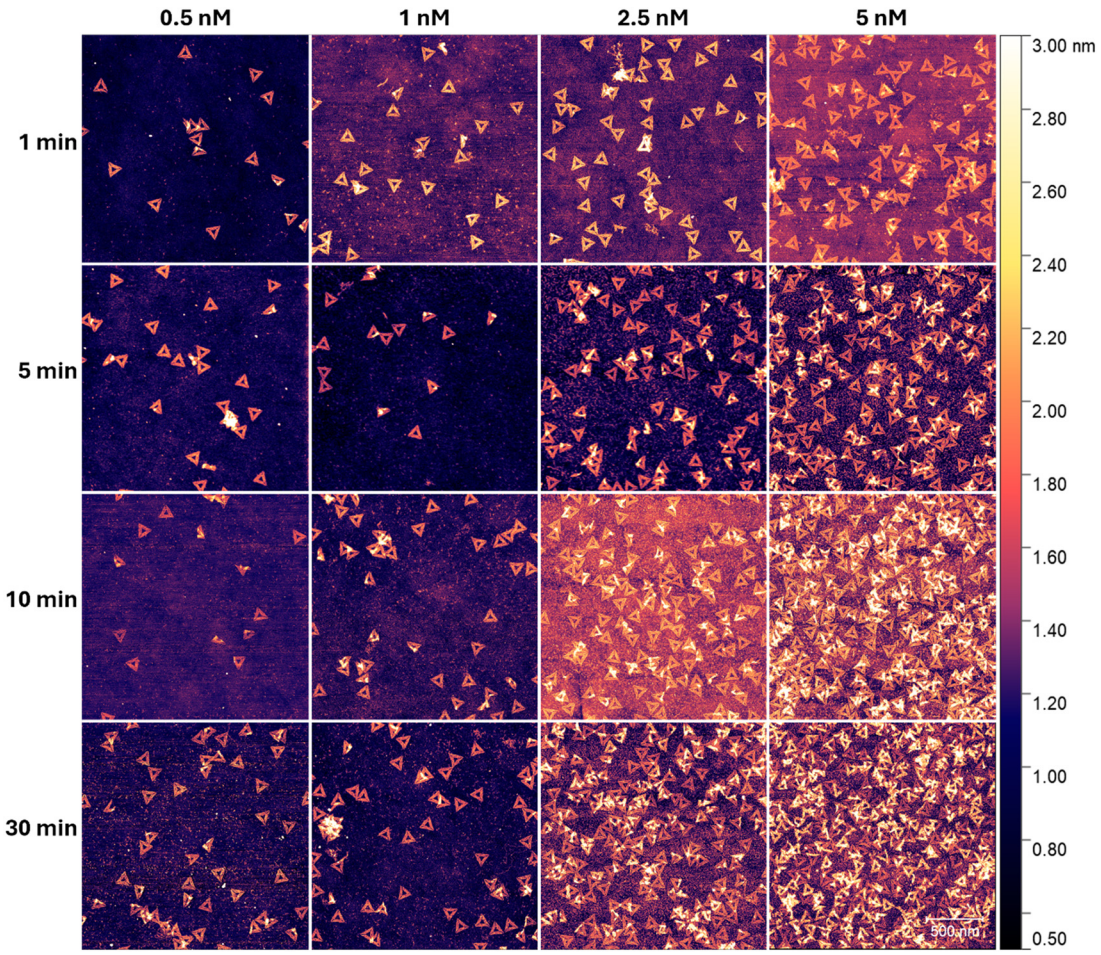

Fig. 1 AFM images (2 × 2 μm^2) of DNA origami triangles adsorbed on TiO_2(001) surfaces in the presence of 5 mM Mg^{2+}. The DNA origami concentrations and incubation times are indicated.

Fig. 1 shows AFM images of DNA origami nanostructures adsorbed at TiO_2(001) in the presence of 5 mM Mg^{2+}. At constant DNA origami concentration, longer incubation times in general lead to a larger DNA origami surface coverage. The same is observed at a fixed incubation time upon increasing the DNA origami concentration. For DNA origami concentrations of 2.5 nM and higher, this leads to the formation of multilayers at incubation times exceeding 5 min.

Interestingly, increasing the Mg^{2+} concentration to 10 mM does not result in any strong variations in the overall trends (see Fig. 2). However, upon close inspection of the corresponding AFM images, it appears that for long incubation times and high DNA origami concentrations (such as 30 min at 5 nM), the obtained surface coverage is slightly decreased at 10 mM Mg^{2+}. This behavior is rather surprising because for SiO_2 surfaces, which also are negatively charged in 1× TAE buffer, higher Mg^{2+} concentrations usually result in larger surface coverage.[26,30]

For better comparison, the surface coverage after DNA origami adsorption was calculated for each condition and is presented in Fig. 3. As can be seen, the overall trends visually observed in the AFM images are well reproduced in the quantitative data. Increasing both incubation time and DNA origami concentration leads to higher surface coverage. More importantly, however, the data in Fig. 3 also reveals that the

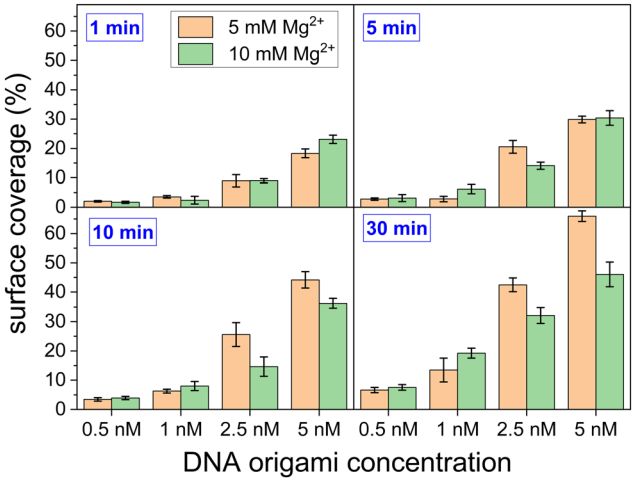

Fig. 3 DNA origami surface coverage on the TiO_2(001) surface at different conditions. Values represent averages over 3 to 12 AFM images recorded at different positions on the surfaces. Error bars represent the standard deviations. See Fig. S4–S35† for the thresholded images.

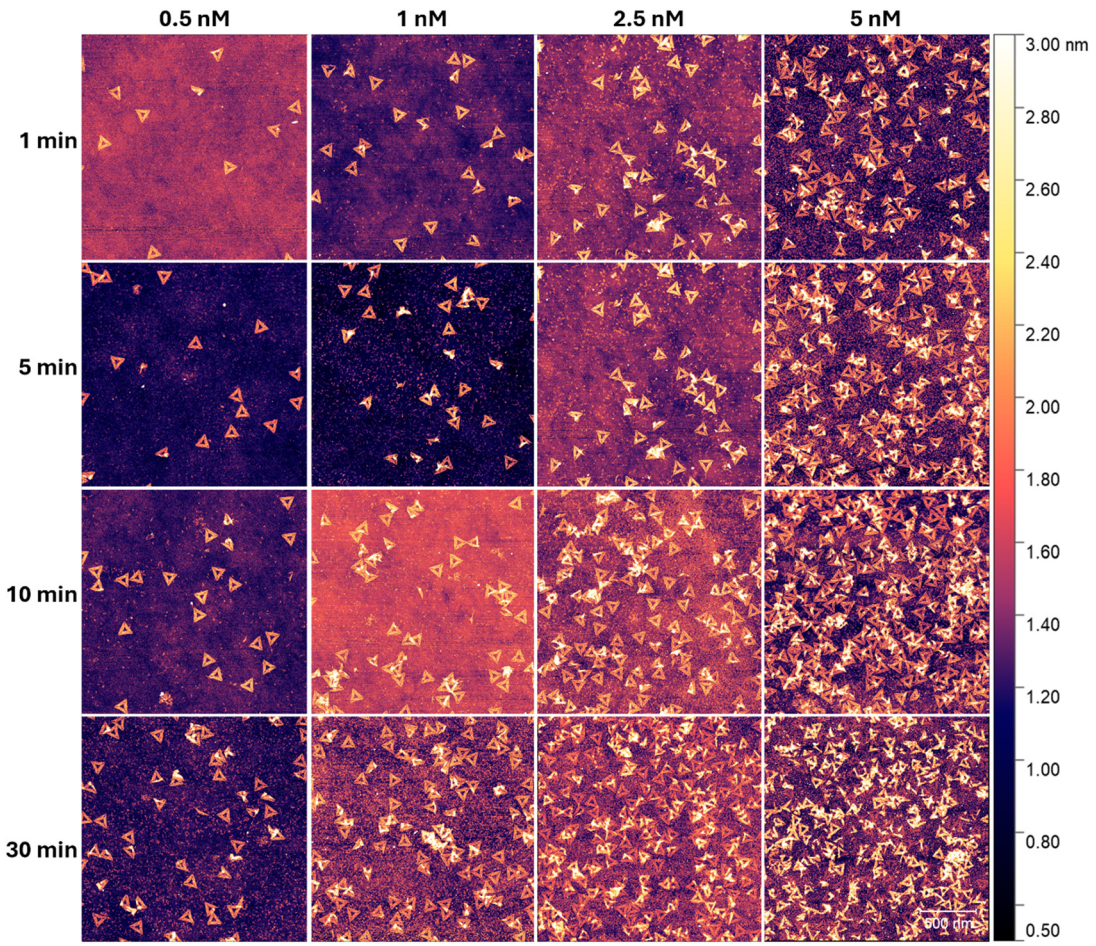

Fig. 2 AFM images (2 × 2 μm^2) of DNA origami triangles adsorbed on TiO_2(001) surfaces in the presence of 10 mM Mg^{2+}. The DNA origami concentrations and incubation times are indicated.

differences in the surface coverage obtained for the different Mg^{2+} concentrations depend on incubation time and DNA origami concentration. At short incubation times below 10 min and low DNA origami concentrations below 2.5 nM, the Mg^{2+} concentration does not have a pronounced effect on surface coverage. At high DNA origami concentrations and long incubation times, however, the surface coverage obtained in the presence of 5 mM Mg^{2+} is notably higher than that obtained at 10 mM Mg^{2+}. Under these conditions, the increase in surface coverage due to the reduction in Mg^{2+} concentration ranges from 22 to 75% with no notable trend.

Next, we sought to investigate whether this peculiar effect of the Mg^{2+} concentration is universal for TiO_2. Therefore, we performed additional experiments with alternative substrates. DNA origami triangles were incubated in both Mg^{2+} concentrations also on TiO_2(110) and TiO_2(111) surfaces under conditions that on TiO_2(001) resulted in higher adsorption at 5 mM Mg^{2+}, *i.e.*, 2.5 nM DNA origami triangles incubated for 10 min. For comparison, a silicon wafer with native surface oxide was used as a substrate for adsorption as well. The corresponding AFM images in Fig. 4 reveal a different trend for TiO_2(110) and TiO_2(111). Here, more DNA origami triangles are adsorbed at 10 mM Mg^{2+} than at 5 mM. In contrast, no apparent differences between the two Mg^{2+} concentrations are observed for the SiO_2 surface.

These qualitative observations are substantiated by the calculated surface coverage (Fig. 5). For both the TiO_2(110) and the TiO_2(111) surface, the obtained surface coverage increases by about 34% upon increasing the Mg^{2+} concentrations from 5 mM to 10 mM. For the SiO_2 surface, the two Mg^{2+} concentrations result only in negligible differences. This demonstrates that this peculiar behavior of a lower Mg^{2+} concentration resulting in stronger DNA origami adsorption is specific for the TiO_2(001) surface.

As mentioned above, the IEP of the TiO_2(001) surface lies between 5.5 and 5.8.[67] In contrast, the SiO_2 surface has an IEP around 3.9.[69] Interestingly, the IEP of the TiO_2(110) surface lies in-between those values, *i.e.*, between 4.8 and 5.5.[67] In addition, the TiO_2(001) surface has a lower density of cationic sites than TiO_2(110), *i.e.*, 4.8 *vs.* 6.0 nm^{-2}.[67] For the TiO_2(111) surface, the situation is more complex as this surface is composed of two different domains with cation densities of 3.5 and 5.3 nm^{-2}, respectively.[70] Because of these differences, it has been observed before that the adsorption rates of various ions on single-crystalline TiO_2 surfaces depend on the crystal orientation.[71–73] Therefore, we assume that the observed differences in the influence of Mg^{2+} concentration on DNA origami adsorption are rooted in an orientation-dependence of Mg^{2+} adsorption.

To verify this hypothesis, we have analyzed the chemical composition of the three TiO_2 surfaces after the cleaning procedure by XPS (see Fig. S42 and S43†). The results reveal

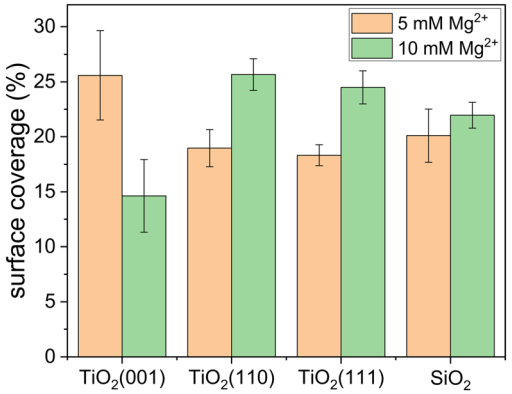

Fig. 5 DNA origami surface coverage on the different TiO_2 and the SiO_2 surfaces after 10 min adsorption of 2.5 nM DNA origami triangles in the presence of 5 mM and 10 mM Mg^{2+}, respectively. Values represent averages over 3 to 12 AFM images recorded at different positions on the surfaces. Error bars represent the standard deviations. See Fig. S22, S26, and S36–S41† for examples of the thresholded images.

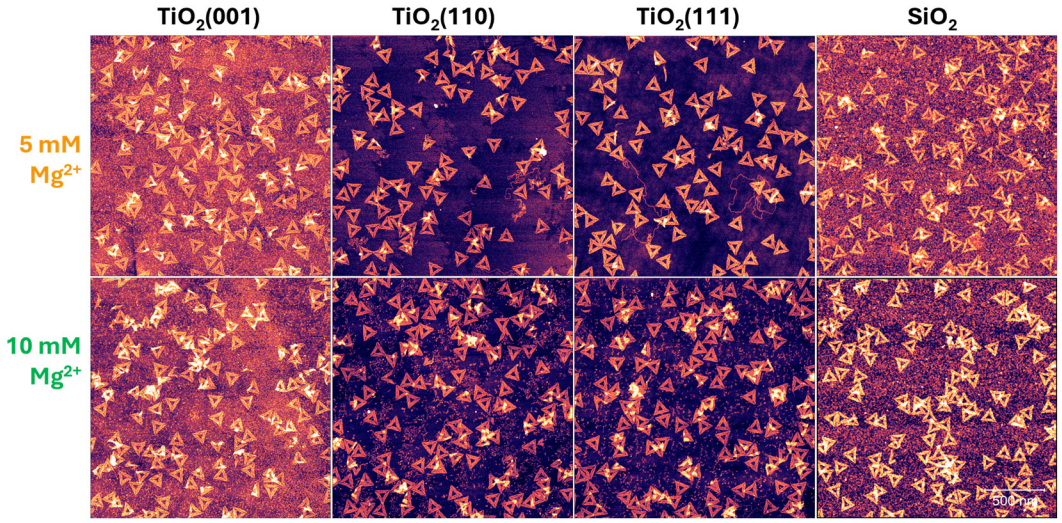

Fig. 4 AFM images (2 × 2 μm^2) of DNA origami triangles (2.5 nM) adsorbed in the presence of 5 mM and 10 mM Mg^{2+}, respectively, at TiO_2(001), TiO_2(110), TiO_2(111), and SiO_2 for 10 min.

Table 1 O 1s : Ti 2p ratios and O 1s surface : bulk (S : B) ratios of the three TiO_2 surfaces as determined by XPS

	TiO_2(001)	TiO_2(110)	TiO_2(111)
O 1s : Ti 2p	3.4	2.3	2.5
O 1s S : B	1.1	0.6	0.7

that the TiO_2(001) surface indeed exhibits a higher fraction of surface oxygens than the other two surfaces, as observed in both the O 1s : Ti 2p ratio and the O 1s surface : bulk ratio (see Table 1). This is in agreement with previous observations and can be attributed to the fact that the TiO_2(001) surface has a low stability and undergoes extensive reconstruction.[67]

Adsorption of negatively charged DNA origami nanostructures at the negatively charged TiO_2 surfaces is controlled by the interplay of Mg^{2+} adsorption at the surface and Mg^{2+} binding to the DNA backbone phosphates. Efficient adsorption requires Mg^{2+} ions to bind simultaneously to a phosphate group and a negative surface charge. Maximum DNA origami adsorption is observed when this condition is met for all phosphate groups in contact with the surface. For the TiO_2(001) surface, the higher fraction of surface oxygens results in an increased basicity, which in turn leads to stronger Mg^{2+} adsorption. Therefore, surface saturation with Mg^{2+} is observed already at a concentration of 5 mM. While a higher Mg^{2+} concentration of 10 mM will not reduce the Mg^{2+} surface coverage, it will lead to more Mg^{2+} ions binding to the DNA phosphate groups already in bulk solution. Upon DNA origami adsorption, this leads to electrostatic repulsion between phosphate-bound and surface-bound Mg^{2+} ions and thus to a lower surface coverage. In this picture, the TiO_2(110) and TiO_2(111) surfaces adsorb fewer Mg^{2+} ions than the TiO_2(001) surface at the same Mg^{2+} concentration. This was verified by XPS, which revealed that after 10 min exposure to 5 mM $MgCl_2$ solution, the TiO_2(110) surface exhibits an about three times lower concentration of adsorbed Mg^{2+} than the TiO_2(001) surface (see Fig. S44†). This reduced Mg^{2+} adsorption results in an insufficient density of salt bridges, so that electrostatic repulsion between the negatively charged phosphate groups and the negative surface charges weakens DNA origami adsorption. At 10 mM, however, a higher number of phosphate groups already carry Mg^{2+} ions that upon adsorption can form salt bridges with the still unoccupied negative surface charges. At still higher Mg^{2+} concentrations, also those TiO_2 surfaces will get saturated with adsorbed Mg^{2+} ions, which then again hinders adsorption. However, at such high Mg^{2+} concentrations, complete charge neutralization and partial charge inversion of the DNA origami nanostructures may occur and lead to DNA origami aggregation.[74,75]

Conclusions

In summary, we have investigated the adsorption of DNA origami triangles at single-crystalline TiO_2 surfaces at different Mg^{2+} concentrations in dependence of incubation time and DNA origami concentration. The surface coverage of the adsorbed DNA origami triangles was quantified by AFM. While our results show that the DNA origami surface coverage on the TiO_2(001) surface increases with incubation time and DNA origami concentration, they also reveal that maximum surface coverage at high DNA origami concentrations and long incubation times is achieved at a rather low Mg^{2+} concentration of 5 mM. At a higher Mg^{2+} concentration of 10 mM, surface coverage is reduced considerably. Intriguingly, this behavior is observed only for the TiO_2(001) surface, whereas for the TiO_2(110) and TiO_2(111) surfaces, maximum surface coverage is observed at 10 mM Mg^{2+}. We attribute this peculiar behavior of the TiO_2(001) surface to the interplay between Mg^{2+} adsorption at the surface and Mg^{2+} binding to the DNA phosphates. Efficient DNA origami adsorption requires a large number of salt bridges at the DNA–TiO_2 interface in the form of Mg^{2+} ions that are bound to both a DNA phosphate and a negatively charged surface site. If the Mg^{2+} concentration is too high, phosphates and surface sites will be both occupied by Mg^{2+} ions, introducing electrostatic repulsion. At the TiO_2(001) surface with its higher basicity, this situation occurs at lower Mg^{2+} concentrations than at the TiO_2(110) and TiO_2(111) surfaces. Our results thus demonstrate that DNA origami surface coverage at different TiO_2 surfaces can be controlled precisely by careful adjustments of the Mg^{2+} concentration, which has important implications for various applications as the electrochemical and photochemical reactivity of TiO_2 is known to depend on its surface orientation.[76,77] However, the same general mechanism may also play a role in the adsorption of DNA origami nanostructures at other single-crystalline oxide surfaces.

Data availability

Data for this article, *i.e.*, raw AFM images and XPS spectra, are available at Zenodo at **https://doi.org/10.5281/zenodo.15369685**.

Author contributions

Xiaodan Xu: methodology, validation, formal analysis, investigation, visualization, writing – original draft, writing – review and editing; Sandra Gołębiowska: formal analysis, investigation, visualization, writing – review and editing; Teresa de los Arcos: formal analysis, writing – review and editing, supervision; Guido Grundmeier: conceptualization, resources, writing – review and editing, supervision; Adrian Keller: conceptualization, methodology, writing – review and editing, supervision.

Conflicts of interest

There are no conflicts to declare.

References

1 P. W. K. Rothemund, Folding DNA to create nanoscale shapes and patterns, *Nature*, 2006, **440**, 297–302.
2 M. Dass, F. N. Gür, K. Kołątaj, M. J. Urban and T. Liedl, DNA Origami-Enabled Plasmonic Sensing, *J. Phys. Chem. C*, 2021, **125**, 5969–5981.
3 M. Loretan, I. Domljanovic, M. Lakatos, C. Rüegg and G. P. Acuna, DNA Origami as Emerging Technology for the Engineering of Fluorescent and Plasmonic-Based Biosensors, *Materials*, 2020, **13**, 2185.
4 E. Sameiyan, E. Bagheri, M. Ramezani, M. Alibolandi, K. Abnous and S. M. Taghdisi, DNA origami-based aptasensors, *Biosens. Bioelectron.*, 2019, **143**, 111662.
5 S. Wang, Z. Zhou, N. Ma, S. Yang, K. Li, C. Teng, Y. Ke and Y. Tian, DNA Origami-Enabled Biosensors, *Sensors*, 2020, **20**, 6899.
6 S. Nummelin, J. Kommeri, M. A. Kostiainen and V. Linko, Evolution of Structural DNA Nanotechnology, *Adv. Mater.*, 2018, **30**, 1703721.
7 S. Dey, C. Fan, K. V. Gothelf, J. Li, C. Lin, L. Liu, N. Liu, M. A. D. Nijenhuis, B. Saccà, F. C. Simmel, H. Yan and P. Zhan, DNA origami, *Nat. Rev. Methods Primers*, 2021, **1**, 13.
8 M. Godonoga, T.-Y. Lin, A. Oshima, K. Sumitomo, M. S. L. Tang, Y.-W. Cheung, A. B. Kinghorn, R. M. Dirkzwager, C. Zhou, A. Kuzuya, J. A. Tanner and J. G. Heddle, A DNA aptamer recognising a malaria protein biomarker can function as part of a DNA origami assembly, *Sci. Rep.*, 2016, **6**, 21266.
9 J. Huang, A. Suma, M. Cui, G. Grundmeier, V. Carnevale, Y. Zhang, C. Kielar and A. Keller, Arranging Small Molecules with Subnanometer Precision on DNA Origami Substrates for the Single-Molecule Investigation of Protein–Ligand Interactions, *Small Struct.*, 2020, **1**, 2000038.
10 X. Ouyang, M. de Stefano, A. Krissanaprasit, A. L. Bank Kodal, C. Bech Rosen, T. Liu, S. Helmig, C. Fan and K. V. Gothelf, Docking of Antibodies into the Cavities of DNA Origami Structures, *Angew. Chem., Int. Ed.*, 2017, **56**, 14423–14427.
11 V. Linko, M. Eerikäinen and M. A. Kostiainen, A modular DNA origami-based enzyme cascade nanoreactor, *Chem. Commun.*, 2015, **51**, 5351–5354.
12 Y. Choi, L. Kotthoff, L. Olejko, U. Resch-Genger and I. Bald, DNA Origami-Based Förster Resonance Energy-Transfer Nanoarrays and Their Application as Ratiometric Sensors, *ACS Appl. Mater. Interfaces*, 2018, **10**, 23295–23302.
13 J. Prinz, C. Heck, L. Ellerik, V. Merk and I. Bald, DNA origami based Au-Ag-core-shell nanoparticle dimers with single-molecule SERS sensitivity, *Nanoscale*, 2016, **8**, 5612–5620.
14 Y. Huang, M.-K. Nguyen, A. K. Natarajan, V. H. Nguyen and A. Kuzyk, A DNA Origami-Based Chiral Plasmonic Sensing Device, *ACS Appl. Mater. Interfaces*, 2018, **10**, 44221–44225.
15 D. Huang, L. Haddad, F. Rahman, M. Palma and A. Sapelkin, Engineering a DNA origami mediated multicolour quantum dot platform for sub-diffraction spectral separation imaging, *RSC Adv.*, 2022, **12**, 23778–23785.
16 T. Zhang, A. Neumann, J. Lindlau, Y. Wu, G. Pramanik, B. Naydenov, F. Jelezko, F. Schüder, S. Huber, M. Huber, F. Stehr, A. Högele, T. Weil and T. Liedl, DNA-Based Self-Assembly of Fluorescent Nanodiamonds, *J. Am. Chem. Soc.*, 2015, **137**, 9776–9779.
17 S. E. Ochmann, C. Vietz, K. Trofymchuk, G. P. Acuna, B. Lalkens and P. Tinnefeld, Optical Nanoantenna for Single Molecule-Based Detection of Zika Virus Nucleic Acids without Molecular Multiplication, *Anal. Chem.*, 2017, **89**, 13000–13007.
18 K. Tapio, A. Mostafa, Y. Kanehira, A. Suma, A. Dutta and I. Bald, A Versatile DNA Origami-Based Plasmonic Nanoantenna for Label-Free Single-Molecule Surface-Enhanced Raman Spectroscopy, *ACS Nano*, 2021, **15**, 7065–7077.
19 D. Daems, W. Pfeifer, I. Rutten, B. Saccà, D. Spasic and J. Lammertyn, Three-Dimensional DNA Origami as Programmable Anchoring Points for Bioreceptors in Fiber Optic Surface Plasmon Resonance Biosensing, *ACS Appl. Mater. Interfaces*, 2018, **10**, 23539–23547.
20 P. Williamson, P. Piskunen, H. Ijäs, A. Butterworth, V. Linko and D. K. Corrigan, Signal Amplification in Electrochemical DNA Biosensors Using Target-Capturing DNA Origami Tiles, *ACS Sens.*, 2023, **8**, 1471–1480.
21 T. Zheng, C. O'Neill, J. F. Marshall, T. Iskratsch and M. Palma, Selective placement of functionalised DNA origami via thermal scanning probe lithography patterning, *Mater. Adv.*, 2024, **5**, 9376–9382.
22 J. M. Yun, K. N. Kim, J. Y. Kim, D. O. Shin, W. J. Lee, S. H. Lee, M. Lieberman and S. O. Kim, DNA origami nanopatterning on chemically modified graphene, *Angew. Chem., Int. Ed.*, 2012, **51**, 912–915.
23 B. Teshome, S. Facsko and A. Keller, Topography-controlled alignment of DNA origami nanotubes on nanopatterned surfaces, *Nanoscale*, 2014, **6**, 1790–1796.
24 B. Teschome, S. Facsko, K. V. Gothelf and A. Keller, Alignment of Gold Nanoparticle-Decorated DNA Origami Nanotubes: Substrate Prepatterning versus Molecular Combing, *Langmuir*, 2015, **31**, 12823–12829.
25 K. Tapio, C. Kielar, J. M. Parikka, A. Keller, H. Järvinen, K. Fahmy and J. J. Toppari, Large-Scale Formation of DNA Origami Lattices on Silicon, *Chem. Mater.*, 2023, **35**, 1961–1971.
26 S. Takabayashi, S. Kotani, J. Flores-Estrada, E. Spears, J. E. Padilla, L. C. Godwin, E. Graugnard, W. Kuang, S. Sills and W. L. Hughes, Boron-Implanted Silicon Substrates for Physical Adsorption of DNA Origami, *Int. J. Mol. Sci.*, 2018, **19**, 2513.
27 K. B. Ricardo, A. Xu, M. Salim, F. Zhou and H. Liu, Deposition of DNA Nanostructures on Highly Oriented Pyrolytic Graphite, *Langmuir*, 2017, **33**, 3991–3997.
28 B. K. Pothineni, C. Theile-Rasche, H. Müller, G. Grundmeier, T. de Los Arcos and A. Keller, DNA Origami Adsorption and Lattice Formation on Different SiOx Surfaces, *Chem. – Eur. J.*, 2025, e202404108.

29 Y. Gao, J. Chen, J. Liu, M. Li and Y. Wang, Deposition of DNA Nanostructures on Highly Oriented Pyrolytic Graphite, *Adv. Mater. Interfaces*, 2025, **12**, 2400557.
30 K. Brassat, S. Ramakrishnan, J. Bürger, M. Hanke, M. Doostdar, J. K. N. Lindner, G. Grundmeier and A. Keller, On the Adsorption of DNA Origami Nanostructures in Nanohole Arrays, *Langmuir*, 2018, **34**, 14757–14765.
31 B. K. Pothineni, G. Grundmeier and A. Keller, Cation-dependent assembly of hexagonal DNA origami lattices on SiO2 surfaces, *Nanoscale*, 2023, **15**, 12894–12906.
32 A. Fujishima and K. Honda, Electrochemical Photolysis of Water at a Semiconductor Electrode, *Nature*, 1972, **238**, 37.
33 A. Fujishima, K. Kohayakawa and K. Honda, Hydrogen Production under Sunlight with an Electrochemical Photocell, *J. Electrochem. Soc.*, 1975, **122**, 1487–1489.
34 J. Nowotny, T. Bak, M. K. Nowotny and L. R. Sheppard, TiO2 surface active sites for water splitting, *J. Phys. Chem. B*, 2006, **110**, 18492–18495.
35 J. Low, B. Cheng and J. Yu, Surface modification and enhanced photocatalytic CO2 reduction performance of TiO2: a review, *Appl. Surf. Sci.*, 2017, **392**, 658–686.
36 O. Ola and M. Maroto-Valer, Review of material design and reactor engineering on TiO2 photocatalysis for CO2 reduction, *J. Photochem. Photobiol., C*, 2015, **24**, 16–42.
37 N. Shehzad, M. Tahir, K. Johari, T. Murugesan and M. Hussain, A critical review on TiO2 based photocatalytic CO2 reduction system: Strategies to improve efficiency, *J. CO2 Util.*, 2018, **26**, 98–122.
38 S. S. Mani, S. Rajendran, T. Mathew and C. S. Gopinath, A review on the recent advances in the design and structure–activity relationship of TiO 2-based photocatalysts for solar hydrogen production, *Energy Adv.*, 2024, **3**, 1472–1504.
39 J. Gao, S. Wang, H. Cai, S. Chen, L. Zheng, Y. Li and G. He, Portable photocatalytic fuel cell with anatase/rutile TiO_2 heterophase junction for solar energy harvesting and pollutant degradation, *Int. J. Hydrogen Energy*, 2025, **97**, 259–269.
40 J. Zhao, H. Wang, Y. Cai, J. Zhao, Z. Gao and Y.-Y. Song, The Challenges and Opportunities for TiO2 Nanostructures in Gas Sensing, *ACS Sens.*, 2024, **9**, 1644–1655.
41 J. Bai and B. Zhou, Titanium dioxide nanomaterials for sensor applications, *Chem. Rev.*, 2014, **114**, 10131–10176.
42 L. Bertel, D. A. Miranda and J. M. García-Martín, Nanostructured Titanium Dioxide Surfaces for Electrochemical Biosensing, *Sensors*, 2021, **21**, 6167.
43 Y. Xin, G. Grundmeier and A. Keller, Adsorption of SARS-CoV-2 Spike Protein S1 at Oxide Surfaces Studied by High-Speed Atomic Force Microscopy, *Adv. NanoBiomed Res.*, 2021, **1**, 2000024.
44 Y. Yang, S. Knust, S. Schwiderek, Q. Qin, Q. Yun, G. Grundmeier and A. Keller, Protein Adsorption at Nanorough Titanium Oxide Surfaces: The Importance of Surface Statistical Parameters beyond Surface Roughness, *Nanomaterials*, 2021, **11**, 357.
45 J. E. Ellingsen, A study on the mechanism of protein adsorption to TiO2, *Biomaterials*, 1991, **12**, 593–596.
46 B. E. Givens, Z. Xu, J. Fiegel and V. H. Grassian, Bovine serum albumin adsorption on SiO2 and TiO2 nanoparticle surfaces at circumneutral and acidic pH: A tale of two nano-bio surface interactions, *J. Colloid Interface Sci.*, 2017, **493**, 334–341.
47 Y. Kang, X. Li, Y. Tu, Q. Wang and H. Ågren, On the Mechanism of Protein Adsorption onto Hydroxylated and Nonhydroxylated TiO 2 Surfaces, *J. Phys. Chem. C*, 2010, **114**, 14496–14502.
48 S. R. Sousa, P. Moradas-Ferreira, B. Saramago, L. V. Melo and M. A. Barbosa, Human serum albumin adsorption on TiO2 from single protein solutions and from plasma, *Langmuir*, 2004, **20**, 9745–9754.
49 Z. Xu and V. H. Grassian, Bovine Serum Albumin Adsorption on TiO 2 Nanoparticle Surfaces: Effects of pH and Coadsorption of Phosphate on Protein–Surface Interactions and Protein Structure, *J. Phys. Chem. C*, 2017, **121**, 21763–21771.
50 A. G. Hemmersam, M. Foss, J. Chevallier and F. Besenbacher, Adsorption of fibrinogen on tantalum oxide, titanium oxide and gold studied by the QCM-D technique, *Colloids Surf., B*, 2005, **43**, 208–215.
51 N. A. Parmin, U. Hashim, S. C. B. Gopinath, S. Nadzirah, Z. Rejali, A. Afzan, M. N. A. Uda, V. C. Hong and R. D. A. A. Rajapaksha, Voltammetric determination of human papillomavirus 16 DNA by using interdigitated electrodes modified with titanium dioxide nanoparticles, *Microchim. Acta*, 2019, **186**, 336.
52 S. Nadzirah, U. Hashim, S. C. B. Gopinath, N. A. Parmin, A. A. Hamzah, H. W. Yu and C. F. Dee, Titanium dioxide-mediated resistive nanobiosensor for E. coli O157:H7, *Microchim. Acta*, 2020, **187**, 235.
53 W. Lu, G. Wang, Y. Jin, X. Yao, J. Hu and J. Li, Label-free photoelectrochemical strategy for hairpin DNA hybridization detection on titanium dioxide electrode, *Appl. Phys. Lett.*, 2006, **89**, 263902.
54 W. Lu, Y. Jin, G. Wang, Da Chen and J. Li, Enhanced photoelectrochemical method for linear DNA hybridization detection using Au-nanopaticle labeled DNA as probe onto titanium dioxide electrode, *Biosens. Bioelectron.*, 2008, **23**, 1534–1539.
55 Y. Kim and S. K. Mohanty, PNA Functionalized Gold Nanoparticles on TiO 2 Nanotubes Biosensor for Electrochemical DNA Fragment Detection, *Adv. Mater. Interfaces*, 2025, 2400762.
56 W. Ding, C. Song, T. Li, H. Ma, Y. Yao and C. Yao, TiO2 nanowires as an effective sensing platform for rapid fluorescence detection of single-stranded DNA and double-stranded DNA, *Talanta*, 2019, **199**, 442–448.
57 B. Baykal, G. Kadikoylu, H. Senturk, Y. O. Donar, A. Sınağ and A. Erdem, Preparation and characterization gallic acid-titanium dioxide nanocomposites for biosensing application on voltammetric detection of DNA, *J. Electroanal. Chem.*, 2021, **892**, 115262.

58 J. Yoo, H. Jeong, S. K. Park, S. Park and J. S. Lee, Interdigitated Electrode Biosensor Based on Plasma-Deposited TiO2 Nanoparticles for Detecting DNA, *Biosensors*, 2021, **11**, 212.
59 T. Amano, T. Toyooka and Y. Ibuki, Preparation of DNA-adsorbed TiO2 particles–augmentation of performance for environmental purification by increasing DNA adsorption by external pH regulation, *Sci. Total Environ.*, 2010, **408**, 480–485.
60 H. Suzuki, T. Amano, T. Toyooka and Y. Ibuki, Preparation of DNA-adsorbed TiO2 particles with high performance for purification of chemical pollutants, *Environ. Sci. Technol.*, 2008, **42**, 8076–8082.
61 C. Kielar, Y. Xin, B. Shen, M. A. Kostiainen, G. Grundmeier, V. Linko and A. Keller, On the Stability of DNA Origami Nanostructures in Low-Magnesium Buffers, *Angew. Chem., Int. Ed.*, 2018, **57**, 9470–9474.
62 F. Kollmann, S. Ramakrishnan, B. Shen, G. Grundmeier, M. A. Kostiainen, V. Linko and A. Keller, Superstructure-Dependent Loading of DNA Origami Nanostructures with a Groove-Binding Drug, *ACS Omega*, 2018, **3**, 9441–9448.
63 W.-J. Kim, S. Kim, B. S. Lee, A. Kim, C. S. Ah, C. Huh, G. Y. Sung and W. S. Yun, Enhanced protein immobilization efficiency on a TiO2 surface modified with a hydroxyl functional group, *Langmuir*, 2009, **25**, 11692–11697.
64 *Handbook of Silicon Wafer Cleaning Technology*, ed. K. A. Reinhardt and W. Kern, William Andrew Publishing, 3rd edn, 2018.
65 D. Nečas and P. Klapetek, Gwyddion: an open-source software for SPM data analysis, *Open Phys.*, 2012, **10**, 181–188.
66 E. Usenko, A. Glamazda, A. Svidzerska, V. Valeev, A. Laguta, S. Petrushenko and V. Karachevtsev, DNA:TiO2 nanoparticle nanoassemblies: effect of temperature and nanoparticle concentration on aggregation, *J. Nanopart. Res.*, 2023, **25**, 113.
67 J. W. Bullard and M. J. Cima, Orientation dependence of the isoelectric point of TiO2 (rutile) surfaces, *Langmuir*, 2006, **22**, 10264–10271.
68 V. Linko and A. Keller, Stability of DNA Origami Nanostructures in Physiological Media: The Role of Molecular Interactions, *Small*, 2023, **19**, e2301935.
69 K. J. Trevino, J. C. Shearer, B. D. Tompkins and E. R. Fisher, Comparing Isoelectric Point and Surface Composition of Plasma Modified Native and Deposited SiO 2 Films Using Contact Angle Titrations and X-ray Photoelectron Spectroscopy, *Plasma Processes Polym.*, 2011, **8**, 951–964.
70 H. Uetsuka, M. A. Henderson, A. Sasahara and H. Onishi, Formate Adsorption on the (111) Surface of Rutile TiO 2, *J. Phys. Chem. B*, 2004, **108**, 13706–13710.
71 A. Hiji, T. Hanawa, T. Yokoi, P. Chen, M. Ashida and M. Kawashita, Time Transient of Calcium and Phosphate Ion Adsorption by Rutile Crystal Facets in Hanks' Solution Characterized by XPS, *Langmuir*, 2021, **37**, 3597–3604.
72 T. Toyoda, W. Yindeesuk, K. Kamiyama, S. Hayase and Q. Shen, Effect of TiO 2 Crystal Orientation on the Adsorption of CdSe Quantum Dots for Photosensitization Studied by the Photoacoustic and Photoelectron Yield Methods, *J. Phys. Chem. C*, 2014, **118**, 16680–16687.
73 T. Toyoda, Q. Shen, K. Hori, N. Nakazawa, K. Kamiyama and S. Hayase, Crystal Growth, Exponential Optical Absorption Edge, and Ground State Energy Level of PbS Quantum Dots Adsorbed on the (001), (110), and (111) Surfaces of Rutile-TiO 2, *J. Phys. Chem. C*, 2018, **122**, 13590–13599.
74 Y. Xin, S. Martinez Rivadeneira, G. Grundmeier, M. Castro and A. Keller, Self-assembly of highly ordered DNA origami lattices at solid-liquid interfaces by controlling cation binding and exchange, *Nano Res.*, 2020, **13**, 3142–3150.
75 L. Opherden, J. Oertel, A. Barkleit, K. Fahmy and A. Keller, Paramagnetic decoration of DNA origami nanostructures by Eu^{3+} coordination, *Langmuir*, 2014, **30**, 8152–8159.
76 R. Hengerer, L. Kavan, P. Krtil and M. Grätzel, Orientation Dependence of Charge-Transfer Processes on TiO[sub 2] (Anatase) Single Crystals, *J. Electrochem. Soc.*, 2000, **147**, 1467.
77 P. A. Morris Hotsenpiller, J. D. Bolt, W. E. Farneth, J. B. Lowekamp and G. S. Rohrer, Orientation Dependence of Photochemical Reactions on TiO 2 Surfaces, *J. Phys. Chem. B*, 1998, **102**, 3216–3226.